FISEVIER

Contents lists available at ScienceDirect

Engineering Fracture Mechanics

journal homepage: www.elsevier.com/locate/engfracmech





Fatigue life prediction of the FCC-based multi-principal element alloys via domain knowledge-based machine learning

Lu Xiao ^a, Gang Wang ^b, Weimin Long ^c, Peter K. Liaw ^d, Jingli Ren ^{a,*}

- ^a Henan Academy of Big Data, Zhengzhou University, Zhengzhou 450052, China
- ^b Institute of Materials, Shanghai University, Shanghai 200444, China
- ^c State Key Laboratory of Advanced Brazing Metals & Technology, Zhengzhou Research Institute of Mechanical Engineering, Zhengzhou 450001, China
- d Department of Materials Science and Engineering, The University of Tennessee, Knoxville, TN 37996, USA

ARTICLE INFO

Keywords: Fatigue life prediction Domain knowledge Machine learning Multi-principal element alloy Small dataset

ABSTRACT

We propose a machine learning (ML) model to predict the fatigue life of multi-principal element alloys (MPEAs) by extracting features from empirical formulas. The model is built on XGBoost and GBDT, and outperforms the single ML model, with almost all predictions lying in the \pm 2 error bands and the relative error not exceeding 0.16 in the extrapolation test. Feature analysis shows that for the nine explored MPEAs systems, their S–N curves are more suitable to be fitted by $\log N = a + b \log \sigma_{max}$. Interpretable analysis indicates that for the explored alloys, elongation > 47% benefits the increase of fatigue life; if their yield strength is less than 720 MPa, improving strength will favor improvement in lifetime, otherwise improving ductility will favor lengthening their lifetime. It provides a fast and low-cost method to predict the fatigue life of those FCC-based MPEAs, which guides designing alloys with longer fatigue life.

1. Introduction

The vast majority of failures in engineering applications are fatigue failures. Fatigue is the phenomenon that a structure fails under cyclic loading below its ultimate strength. Fatigue life refers to the lifetime from service to failure in a given cyclic loading [1]. Actually, fatigue tests are commonly time-consuming and costly. Obtaining each point in the S–N curve may take hours, days, or longer. Therefore, providing reliable material fatigue life prediction before applications and exploring potential factors that affect fatigue life become crucial.

The powerful data mining capabilities of machine learning (ML) have brought effective solutions to various problems [2–4], including the research of material fatigue. Some successful works have been made on conventional materials. For instance, Yang et al. [5] employed four ML algorithms to explore the effect of geometrical size on the fatigue life of A588 steel. Hao et al. [6] proposed a physics-informed ML framework for the fatigue life prediction of aerospace polycrystalline alloys. In addition, based on the small-scale fatigue experimental dataset of Al alloys, Lian et al. [7] proposed a knowledge-based ML framework that extracts features from empirical formulas to construct a model for predicting lifetime.

Unlike conventional materials, multi-principal element alloys (MPEAs) are composed of multiple major elements with equal or near-equal molarity [8]. Their excellent properties have attracted widespread attention from academia and industry [9–12]. Recent experimental explorations have illustrated that MPEAs present outstanding fatigue properties [13–16]. For instance, Lu et al. found that under similar strain amplitudes, the fatigue life of CoCrFeMnNi (Cantor) alloy is longer than that of 316L steel [13], but shorter

https://doi.org/10.1016/j.engfracmech.2024.109860

^{*} Corresponding author.

E-mail address: renjl@zzu.edu.cn (J. Ren).

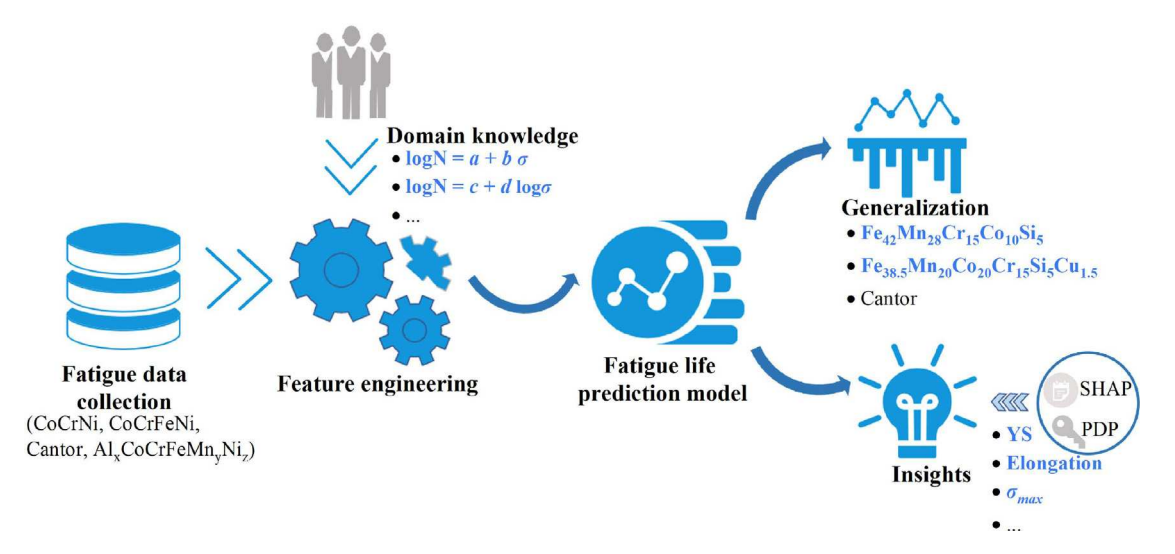


Fig. 1. The flow chart on fatigue life prediction of multi-principal element alloys via domain knowledge-based machine learning.

than that of CoCrNi alloy [14]. At high strain amplitudes, Lu et al. revealed that the fatigue life of dual-phase $Al_{0.5}$ CoCrFeMnNi alloy is shorter than that of Cantor alloy with similar grain sizes [15], and Liu et al. reported that $Fe_{38.5}Mn_{20}Co_{20}Cr_{15}Si_5Cu_{1.5}$ alloy exhibits delayed crack initiation and crack propagation [16].

The applications of ML algorithms in MPEAs mainly focus on two aspects: phase classification and mechanical property prediction [17–19]. In 2023, Sai et al. [20] proposed the pioneering work of fatigue life prediction for MPEAs. They collected 118 data points of $Co_aCr_bFe_cMn_dNi_e$ (68 data points) and $Al_fCo_gCr_hFe_iMn_jNi_k$ (50 data points) systems from the available literature. Based on the small dataset, they used ML algorithms to individually construct regression models for each class of MPEAs, effectively predicting the fatigue life at room temperature.

To date, the available fatigue datasets for specific materials are commonly small, especially for MPEAs whose fatigue behavior has only recently been investigated. However, it is certain that ML models which rely on small datasets are easy to be overfitted [17]. Previous studies have demonstrated that adding prior knowledge to the ML models can effectively prevent overfitting [6,7,21]. Inspired by the work of Sai et al. [20] and Lian et al. [7], we expand the small dataset and then combine empirical formulas to build a voting ML model that can predict the fatigue life of MPEAs. Furthermore, we analyze the factors that affect fatigue life and provide the guidelines for engineering applications.

In this paper, we propose a domain knowledge-based fatigue life prediction model for various MPEA systems. Firstly, 203 fatigue data points are collected from previous literature [13–15,22–39]. Five single ML models are constructed by extracting features from empirical formulas, and then a voting model consisting of the above two best-performing models is built to improve the model's performance. The Shapley Additive exPlanations (SHAP) and partial dependence plot (PDP) are utilized to analyze the quantitative relationship between influencing factors and fatigue life. The overall framework of this work is shown in Fig. 1.

2. Methods

2.1. Data collection

Fatigue datasets of the CoCrNi [14,22], CoCrFeNi [23,24], CoCrFeMnNi [13,25–33], and Al_x CoCrFeMn $_y$ Ni $_z$ [15,34–39] are collected from the available work. The datasets of the above nine FCC-based MPEAs systems are acquired under room temperature fatigue tests with R (minimum/maximum stress) = -1 or 0.1. The fatigue life of the MPEAs systems ranges from 10^2 to 10^7 cycles. The dataset incorporates 28 S–N curves with 203 experimental points, among which one curve from Cantor alloy [13] is selected as the validation set and does not appear in the training set. Each data point includes material chemical composition, mechanical properties, and indicators related to fatigue test. Specifically, the chemical composition is expressed in atomic percentages. Mechanical properties include two stress indicators (yield strength (YS) and ultimate tensile strength (UTS)), and one strain indicator (elongation). The indicators from the fatigue test are composed of stress ratio (R), stress amplitude (σ_a), and the number of cycles to failure (N). The logarithm of fatigue life ($\log N$) is selected as the output target. More details of the original data can be found in the Supplementary file, where Table S1 lists subsets of the dataset, and Fig. S1 shows the distribution of the dataset.

2.2. Feature engineering

2.2.1. Feature generation

Design features based on expert knowledge are effective strategies for improving model performance and overcoming the limitations of small datasets [40]. In general, the S–N curve are fitted by semi-logarithmic or logarithmic mathematical expressions [41]

Table 1

The input features, output variable and their mathematical expression considered in this analysis.

		Descriptors	Description	
Input	Structure descriptors	$a = \sum c_i r_i$	Mean atom radius	
		$\delta = \sqrt{\sum_i c_i (1 - \frac{r_i}{a})^2}$	Atomic size difference	
		$T_m = \sum_{i=1}^{n} c_i T_{mi}$	Average of the melting points of constituent elements	
		$\sigma_T = \sqrt{\sum_i c_i (1 - \frac{T_i}{T_m})^2}$	Standard deviation of melting temperature	
		$\Delta S_{mix} = -K_B \sum_i c_i \ln c_i$	Mixing entropy	
		$\Delta H_{mix} = 4 \sum_{i \neq j} c_i c_j H_{ij}$	Mixing enthalpy	
		$\sigma_{\Delta H} = \sqrt{\sum_{i \neq j} c_i c_j (H_{ij} - \Delta H_{mix})^2}$	Standard deviation of mixing enthalpy	
		$\chi = \sum c_i \chi_i$	Electronegativity	
		$\Delta \chi = \sqrt{\sum c_i (\chi_i - \chi)^2}$	Standard deviation of electronegativity	
		$VEC = \sum c_i VEC_i$	Average VEC	
		$\sigma_{VEC} = \sqrt{\sum c_i (VEC_i - VEC)^2}$	Standard deviation of VEC	
		$K = \sum c_i K_i$	Mean bulk modulus	
		$\sigma_K = \sqrt{\sum c_i (K_i - K)^2}$	Standard deviation of bulk modulus	
	Mechanical properties descriptors	UTS	Ultimate tensile strength	
		YS	Yield strength	
		-	Elongation	
	Parameter of fatigue test	R = minimum/maximum stress	Stress ratio (R)	
		σ_a	Stress amplitude	
		-	descriptors driven from empirical formulas	
Output		$\log_{10} N$	N is the number of cycles to failure	

as follow,

$$\log N = a + b\sigma \tag{1}$$

or

$$\log N = c + d \log \sigma, \tag{2}$$

where σ is σ_a (stress amplitude), σ_{max} (maximum stress), or σ_{min} (minimum stress), and a, b, c, d are coefficients. Therefore, σ_{max} , σ_{min} , $\log \sigma_a$, and $\log \sigma_{max}$ are added to the feature sets.

Fatigue life is also affected by chemical composition, microstructural parameters, and mechanical properties like ultimate tensile strength and yield strength [20,42]. Here, microstructure and chemical composition are not selected as input features as they correlate with mechanical properties and structure descriptors, respectively. The final features and target variable is listed in Table 1.

2.2.2. Feature selection

To eliminate the impact of unit inconsistencies on the performance of ML models, features are firstly normalized as follows,

$$x^* = \frac{x - x_{min}}{x_{max} - x_{min}},\tag{3}$$

where x_{min} and x_{max} are the minimum and maximum values of the feature x, respectively. After normalization, all of the feature values are located at [0, 1].

A good ML model should strike a balance between accuracy and complexity. Thus, redundant features should be removed through the feature selection. Firstly, if there is a strong correlation between multiple features, only one of them is retained. Here, we choose to retain the feature that has a significant impact on model accuracy. Next, all possible combinations of the remaining features are evaluated by exhaustive methods to determine the subset of features with the lowest error (see Supplementary file as Fig. S2 for details). Finally, the $\log \sigma_{max}$, YS, elongation, and σ_K are selected as input features for predicting fatigue life. Fig. 2 plots the Pearson correlation coefficient (ρ) between the four selected features. The $|\rho|$ close to 1 indicate a high correlation between features, while less than 0.8 indicates a weak linear correlation. As evident, there is no strong linear correlation between the four selected features.

2.3. ML algorithms

There is no optimal ML model applicable to all problems. Thus, we exploit five different algorithms, including Extreme Gradient Boosting (XGBoost), Gradient Boosting Decision Tree (GBDT), Random Forest (RF), Support Vector Regression (SVR), and K-Nearest Neighbor (KNN). The hyperparameter values of these algorithms are derived through the grid search method. A brief description and the corresponding hyperparameter values of the above ML algorithms are provided in the Supplementary file. Using the five-fold cross-validation method to measure the performance of all ML models, rather than the traditional strategy of splitting the dataset into training and testing sets. Final results are averaged over 10 random five-fold cross-validations to avoid errors caused by the optimal

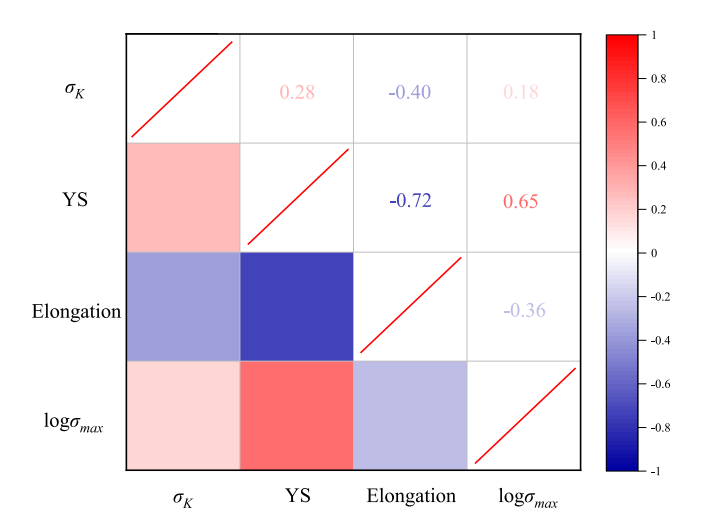


Fig. 2. Pearson correlation coefficient of the selected feature, where the upper triangle represents the ρ-value, and the lower triangle represents the correlation coefficient.

split. The mean absolute error (MAE), mean squared error (MSE), and R-squared (R^2) are used to evaluate the performance of developed prediction models, which are described as:

$$MAE = \frac{1}{n} \sum_{i=1}^{n} |y_i - \hat{y}_i|, \tag{4}$$

$$MSE = \frac{1}{n} \sum_{i=1}^{n} (y_i - \hat{y}_i)^2,$$
 (5)

$$R^{2} = 1 - \frac{\sum_{i=1}^{n} (y_{i} - \hat{y}_{i})^{2}}{\sum_{i=1}^{n} (y_{i} - \bar{y})^{2}},$$
(6)

where y_i , \hat{y}_i , and \bar{y} is the true, prediction, and average values, respectively.

In addition, different algorithms may produce different results for the same problem. Thus, we construct a voting model that concentrates several well-performing algorithms to predict the same problem and uses their average as the final output. The performance of the voting model is evaluated by the above methods.

2.4. Feature analysis

Feature analysis is crucial for extracting useful insights. It could reveal the quantitative and qualitative relationships between features and target variables, thereby providing a more comprehensive understanding. In this paper, the prediction model is interpreted using the game theory-based SHAP [43] method and the PDP [44], a visualization method for black-box explanations, respectively.

3. Results and discussion

3.1. Fatigue life prediction model

The predicted results of five single ML models under the cross-validations strategy are shown in Fig. 3a. By contrast, their accuracy is in the order of GBDT > XGBoost > RF > KNN > SVR. In addition, different algorithms may produce different results for the same problem. Thus, we construct a voting model that concentrates the two best-performing models (GBDT and XGBoost) to predict the same problem and uses their average as the final output. As evident, the voting model exhibits high predictive accuracy than the single ML model with $R^2 = 81.4\%$, MSE = 0.172, and MAE = 0.313.

Fig. 3b shows the predicted and measured fatigue life of the voting model in the training and testing sets split by a ratio of 8:2. It is clear that there is a strong linear relationship between the predicted and measured fatigue life. Moreover, almost all predictions lie in the ± 2 error bands (the pink solid lines), demonstrating the great success of the voting model in predicting fatigue life of the explored MPEAs systems. In addition, only several data points fall between the triple and quadruple error bands. It illustrates that the voting prediction model outperforms previous work, which still has a few data points outside the quadruple error band [20].

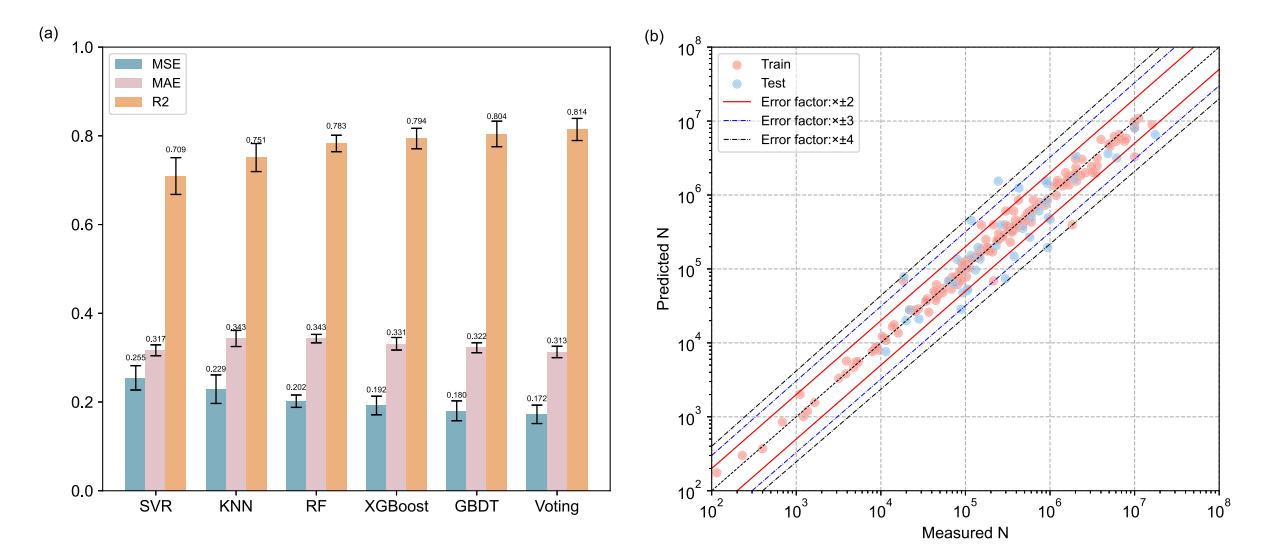


Fig. 3. (a) Mean absolute error (MAE), mean squared error (MSE) and R-squared (R^2) values under the cross-validations strategy for the employed ML algorithms: SVR, KNN, XGBoost, GBDT, RF, and voting model. (b) The plot of experimental vs. predicted fatigue life by the voting model under one split.

3.2. Model explanation analysis

3.2.1. SHAP analysis

The SHAP method is utilized to analyze the influence of the selected features on fatigue life. Due to the limitations of the SHAP method in the voting model, the correlation analysis is conducted on the top-performing GBDT algorithm. As evident from Fig. 4a, the $\log \sigma_{max}$ is the most significant input variable, and the fatigue life is mainly influenced by $\log \sigma_{max}$, YS, and elongation. It is also worth noting that $\log \sigma_{max}$ derived from σ_{max} outweighs other stress features. This trend means the fatigue life of the explored alloys is mainly influenced by σ_{max} rather than σ_a or σ_{min} . Fig. 4b illustrates that the $\log \sigma_{max}$ has a linear contribution with the target variable ($\log N$). It indicates that for the explored MPEAs systems, the σ_{max} -N curve is a better way to describe the relationship between the stress and fatigue life rather than the common σ_a -N curve, i.e., the S–N curve is more suitable to be described by the following logarithmic mathematical expression:

$$\log N = c + d \log \sigma_{max}. \tag{7}$$

Fig. 4c presents that the higher $\log \sigma_{max}$ are associated with larger negative SHAP values, and the smaller $\log \sigma_{max}$ are associated with the larger positive SHAP values. It indicates that the logarithm of the maximum stress is negatively correlated with the target variable. The same trend is displayed in σ_K , while opposite trends can be observed in YS and elongation, which are positively correlated with the target variable. Overall, higher yield strength, great ductility, and smaller standard deviation of bulk modulus favors the increase of fatigue life.

Moreover, we explore the quantitative relation between fatigue life and two influence factors: YS and elongation (see Fig. 4d and e). As shown in Fig. 4d, the explored alloys generally exhibit lower ductility when their yield strength exceeds 720 MPa, but typically have good ductility when their yield strength is below 720 MPa. The YS of 400 MPa and elongation of 47% are critical values, which divide the SHAP values into positive and negative regions. It indicates that YS greater than 400 MPa or elongation greater than 47% is beneficial to lengthen fatigue life. The similar result is also presented in the PDP analysis of YS and elongation (Fig. 4f), that is, alloys with high strength or ductility exhibit good fatigue life.

3.2.2. PDP analysis

As is well known, there is a trade-off relationship between strength and ductility. That means as the alloy's strength increases, its ductility will usually decrease, and vice versa. Therefore, there would exist a turning point during the trade-off process. It can be seen from Fig. 4d that the turning point of 720 MPa divided the explored alloys into two groups: alloys with high strength and alloys with high ductility. So, we explored strategies to improve the fatigue life of these two groups of alloys. The marginal effects of strength and ductility on the predicted fatigue life of the model are analyzed through PDP. The results are displayed in Fig. 5a–e. Here, the X-axis refers to the value of YS or elongation. The Y-axis represents the difference between y_n (the predicted value of the feature at x_n) and y_1 (the predicted value at minimum feature value), which values reflect the effect of improving YS or elongation on fatigue life. The blue shaded area represents the confidence interval, and the solid line denotes the average prediction for all alloys.

Fig. 5a and b indicate that improving YS or elongation of alloys with YS less than 720 MPa will increase their fatigue life. And compared to enhancing lifetime by increasing elongation, increasing YS is a better choice. Fig. 5c and d show that increasing

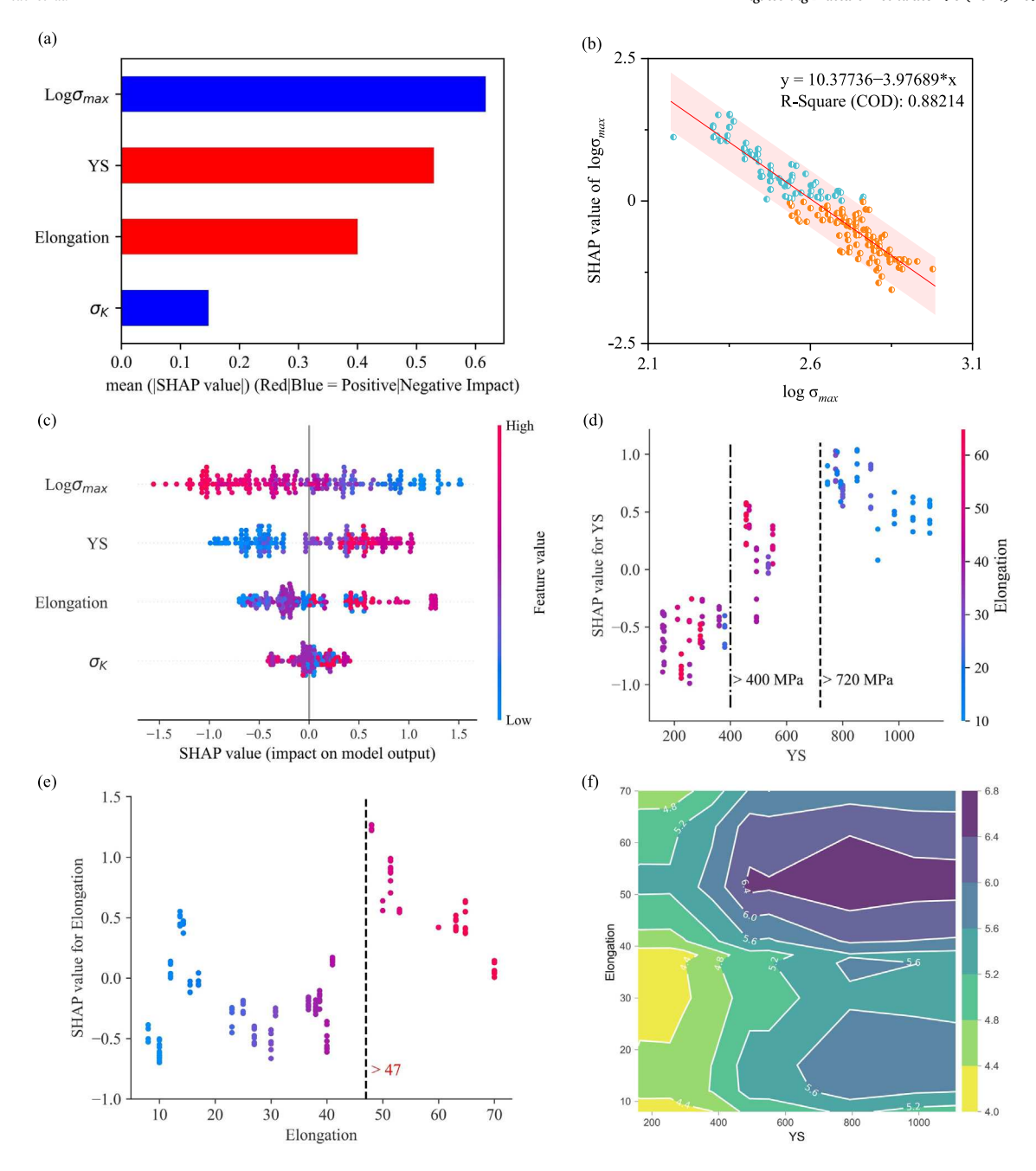


Fig. 4. Feature analysis of SHAP and PDP on GDBT Model. (a) Importance ranking of input features by the mean value of absolute SHAP values. (b) Dependence plot of $log\sigma_{max}$ feature. (c) SHAP value of each input data point. (d) The interaction of YS and elongation for every one of the data by SHAP values. (e) The SHAP values of elongation for every one of the data. (f) The interaction of YS and elongation by PDP.

the elongation of alloys with YS greater than 720 MPa will benefit their lifetime. It is known that simultaneously improving the strength and ductility of alloys is difficult in engineering applications. Thus, when the YS of alloys is less than 720 MPa, increasing their strength is an effective way to improve their fatigue life, otherwise improving enhancing their ductility can effectively extend their lifespan. The existing experimental results validated these findings. Specifically, it is found that alloys with yield strength greater than 720 MPa show no improvement in fatigue properties when enhancing their yield strength, but exhibit excellent fatigue resistance when improving their ductility [34,37]. Refs. [31,33] show that alloy has excellent fatigue resistance when improving yield strength from 300 MPa to 800 MPa and 293.1 MPa to 774.8 MPa, respectively. In addition, the similar results also can be found by comparing the S–N curves obtained under the same experimental conditions [15,23,25,29,36–38]. Specifically, when the alloy's YS is less than 720 MPa, alloys with higher YS exhibit longer fatigue life, as shown in Fig. 6a–c. When their YS is greater

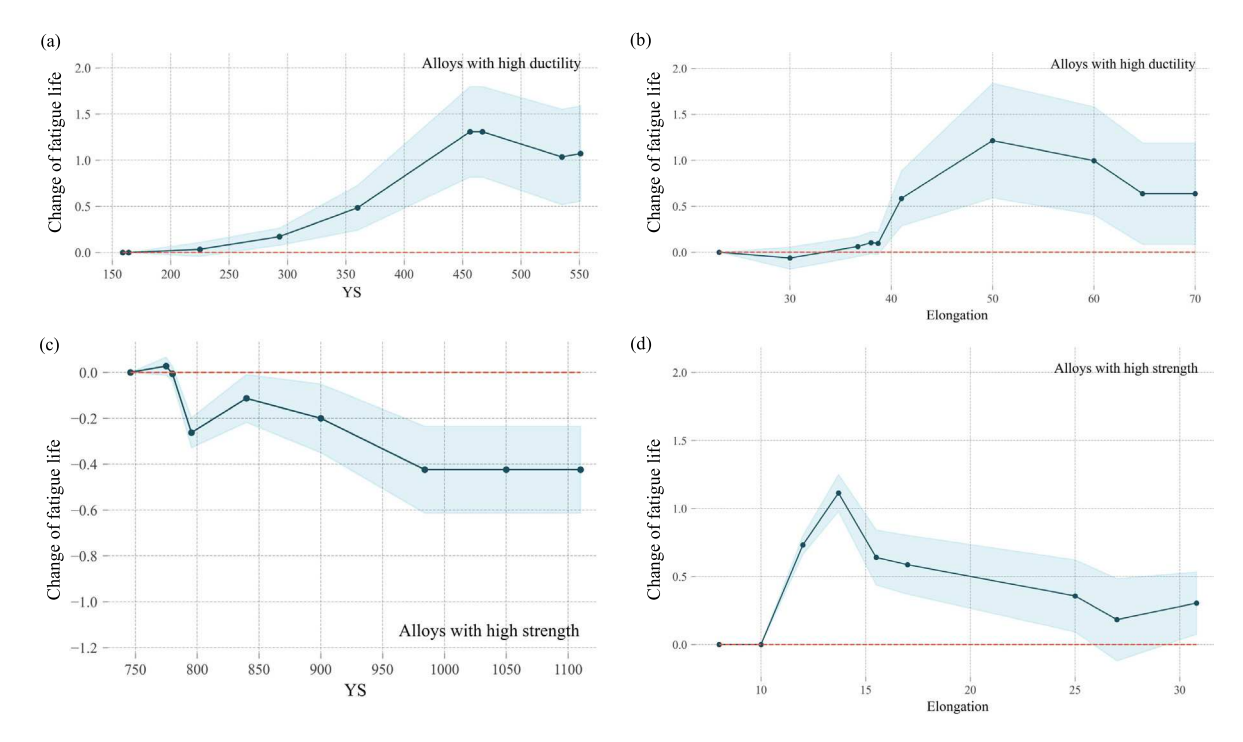


Fig. 5. Partial dependence plot for YS and elongation of two groups of alloys: (a, b) alloys with high ductility, (c, d) alloys with high strength. The X-axis refers to the value of YS or elongation. The Y-axis indicates the effect of improving YS or elongation on fatigue life.

than 720 MPa, the increase in YS will not increase their fatigue life, as shown in Fig. 6d. It provides guidelines for designing alloys with longer fatigue life in engineering applications.

3.3. Evaluation of generalization ability for unexplored alloys

A more practical need in engineering is to evaluate materials that do not appear in the training set. Thus, to verify the generalization ability of the prediction model, experimental data of the Cantor alloys and three new materials: $Fe_{42}Mn_{28}Cr_{15}Co_{10}Si_5$, $Fe_{38.5}Mn_{20}Co_{20}Cr_{15}Si_5Cu_{1.5}$, and HfNbTaTiZr are collected from available literature [13,16,45,46]. Table 2 gives the comparison between predicted values and experimental results. Relative error, defined as $|y_{true} - y_{prediction}|/y_{true}$, is used as a metric function.

It can be seen from Table 2 that the prediction model performs well in the FeMnCoCrNi $_x$ Si $_y$ Cu $_z$ alloys, with a relative error of no more than 0.16. While in the HfNbTaTiZr alloy, the prediction results are not as good as in the FeMnCoCrNi $_x$ Si $_y$ Cu $_z$ alloys. There are two reasons: one is that the explored MPEA system is mostly composed of Al, Co, Cr, Fe, Mn, and Ni elements, and the knowledge learned by the prediction model is mainly about these systems. The other reason is that, the FCC-based alloys and BCC alloys (such as HfNbTaTiZr) experienced different fatigue damage and deformation mechanisms, making the model obtained mainly from FCC-based alloys cannot accurately predict the fatigue life of the HfNbTaTiZr alloy. The two error points of 0.16 and 0.13 in the Cantor alloy are noisy points, as they are inconsistent with the decreasing trend of the S–N curve. It illustrates that the voting model has high prediction accuracy and power generalization ability for commonly explored MPEA systems. We believe that with the enrichment of fatigue data for various MPEA systems, ML models will have a brighter future in predicting their fatigue life.

4. Conclusion

In summary, this work proposes a voting model based on two best-performing models (GBDT and XGBoost) by extracting features from empirical formulas, which can reliably, fast, and low-costly predict the fatigue life of MPEAs. Partial dependence plots and SHAP values are utilized to analyze the quantitative relationship between influencing factors and fatigue life, which provides guidelines for designing alloys with higher fatigue life in engineering applications. Primary findings are described as follows:

- The voting prediction model outperforms the single ML model, with most data points lying in the double error dispersion bands and relative errors not exceeding 0.16 in predicting the lifetime of unexplored MPEA systems. In addition, since most of the fatigue data in this study were collected from MPEAs of FCC-based microstructure, the proposed model is more applicable for predicting the fatigue life of those FCC-based MPEAs.
- The fatigue life of the nine representative MPEA systems is mainly influenced by σ_{max} rather than σ_{min} or σ_a . Moreover, their S–N curves are more suitable to be described by the mathematical expression, viz., $\log N = a + b \log \sigma_{max}$.

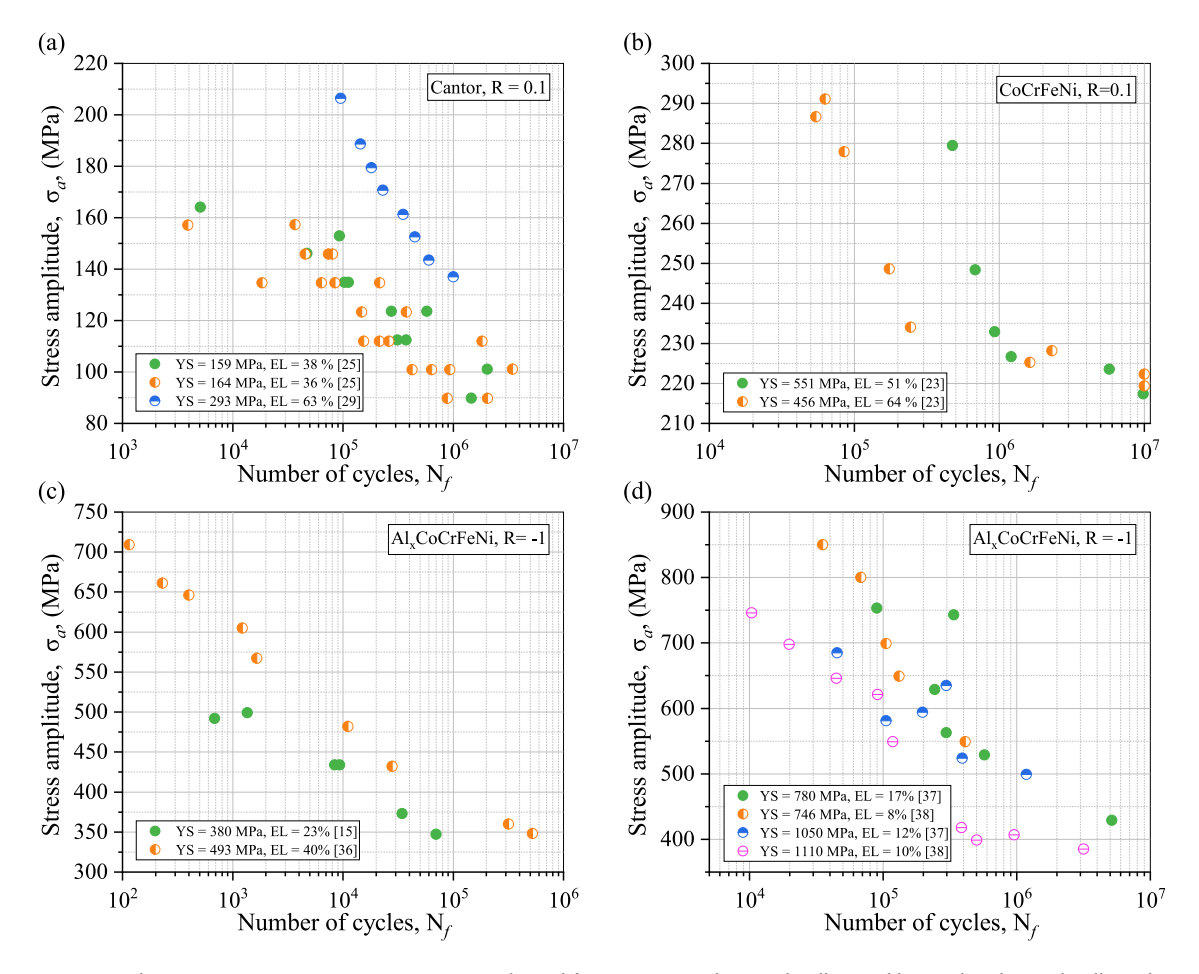


Fig. 6. Comparison between S–N curves in various MPEA systems obtained from previous work. YS is the alloy's yield strength and EL is the alloy's elongation. (a) The S–N curves of Cantor alloy obtained from Ref. [25,29]. (b) The S–N curves of CoCrFeNi alloy obtained from Ref. [23]. (c) The S–N curves of Al_xCoCrFeNi alloy obtained from Ref. [15,36]. (d) The S–N curves of Al_xCoCrFeNi alloy obtained from Ref. [37,38].

• It is found that higher yield strength and ductility favor increasing fatigue life. For the explored alloys, it is better to increase their fatigue life by improving their yield strength instead of ductility when their yield strength is less than 720 MPa; otherwise, improving their ductility for lengthening fatigue life is a better choice.

CRediT authorship contribution statement

Lu Xiao: Writing – original draft, Software, Investigation, Formal analysis. Gang Wang: Writing – review & editing, Validation, Methodology. Weimin Long: Writing – review & editing, Visualization, Validation. Peter K. Liaw: Writing – review & editing, Visualization, Data curation. Jingli Ren: Writing – review & editing, Validation, Supervision, Methodology, Funding acquisition, Conceptualization.

Declaration of competing interest

The authors declare that they have no known competing financial interests or personal relationships that could have appeared to influence the work reported in this paper.

Data availability

Data will be made available on request.

Acknowledgments

This work has been funded by the National Natural Science Foundation of China [Nos. U23A2065, 52071298], and the National Science Foundation, USA [DMR-1611180 and 1809640].

Table 2
Comparison of predicted and experimental fatigue life of the MPEA system.

Alloy	σ_a	$\log N$		
		True	Predict	Relative error
	799.2	4.3	4.5	0.04
	708.6	4.7	4.6	0.02
$Fe_{42}Mn_{28}Cr_{15}Co_{10}Si_{5}$	679.3	5.2	5.1	0.02
	638.9	5.7	5.2	0.09
	577.6	6.5	5.9	0.09
	834.0	4.9	5.3	0.08
Ea Ma Co Ca Si Ca	806.2	5	5.3	0.06
$Fe_{38.5}Mn_{20}Co_{20}Cr_{15}Si_5Cu_{1.5}$	761.9	5	5.3	0.06
	744.9	5.2	5.3	0.02
	433.7	3.4	3.8	0.11
	427.5	3.6	4	0.11
	405.5	3.9	4.2	0.07
CoCrFeMnNi	403.4	3.6	4.3	0.16
Cocrrewiini	385.2	4	4.3	0.07
	384.5	3.8	4.3	0.13
	332.3	4.4	4.9	0.11
	330.7	4.7	4.9	0.04
	514.51	5.4	6.6	0.22
	510.55	4.5	6.7	0.49
	509.77	5.1	6.7	0.31
	507.48	4.6	6.9	0.5
HfNbTaTiZr	503.83	5.2	7	0.35
IIIIVDI di IZI	502.01	5	6.9	0.38
	500.21	5	7	0.4
	499.49	7	7	0
	498.41	7	7.2	0.03
	496.63	7	7.2	0.03

Appendix A. Supplementary data

Supplementary material related to this article can be found online at https://doi.org/10.1016/j.engfracmech.2024.109860.

References

- [1] Kamal M, Rahman MM. Advances in fatigue life modeling: A review. Renew Sustain Energy Rev 2018;82:940-9.
- [2] Rao ZY, Tung PY, Xie RW, Wei Y, Zhang HB, Ferrari A, Klaver TPC, Körmann F, Sukumar PT, da Silva AK, Chen Y, Li ZM, Ponge D, Neugebauer J, Gutfleisch O, Bauer S, Raabe D. Machine learning-enabled high-entropy alloy discovery. Science 2022;378:78–84.
- [3] Vazquez G, Singh P, Sauceda D, Couperthwaite R, Britt N, Youssef K, Johnson DD, Arroyave R. Efficient machine-learning model for fast assessment of elastic properties of high-entropy alloys. Acta Mater 2022;232:117924.
- [4] Wei GY, Cui JZ, Wang W, Guo XX, Ren JL, Wang WH. Short-to-medium range structure and glass-forming ability in metallic glasses. Phys Rev Mater 2022;6:055601.
- [5] Yang WK, Hu BL, Luo YW, Song ZM, Zhang GP. Understanding geometrical size effect on fatigue life of A588 steel using a machine learning approach. Int J Fatigue 2023;172:107671.
- [6] Hao WQ, Tan L, Yang XG, Shi DQ, Wang ML, Miao GL, Fan YS. A physics-informed machine learning approach for notch fatigue evaluation of alloys used in aerospace. Int J Fatigue 2023;170:107536.
- [7] Lian ZH, Li MJ, Lu WC. Fatigue life prediction of aluminum alloy via knowledge-based machine learning. Int J Fatigue 2022;157:106716.
- [8] Yeh JW, Chen SK, Lin SJ, Gan JY, Chin TS, Shun TT, Tsau CH, Chang SY. Nanostructured high-entropy alloys with multiple principal elements: Novel alloy design concepts and outcomes. Adv Energy Mater 2004;6:299–303.
- [9] Fujita K, Tsuboi H, Kikuchi S. Grain size effect on near-threshold fatigue crack propagation in CrMnFeCoNi high-entropy alloy fabricated by spark plasma sintering. Eng Fract Mech 2023;286:109317.
- [10] Liu JP, Guo XX, Lin QY, He ZB, An XH, Li LF, Liaw PK, Liao XZ, Yu LP, Lin JP, Xie L, Ren JL, Zhang Y. Excellent ductility and serration feature of metastable CoCrFeNi high-entropy alloy at extremely low temperatures. Sci China Mater 2019;62:853–63.
- [11] Li YF, Lu CY, Li HX, He YM, Chen GQ, Chen WJ, Zheng WJ, Ma YH, Gao ZL, JG Yang. Uncovering the critical factor governing the fatigue crack propagation under the coexistence of multi-interfaces in AlCoCrFeNi_{2.1} eutectic high-entropy alloy. Eng Fract Mech 2021;258:108132.
- [12] Guo XX, Xie X, Ren JL, Laktionova M, Tabachnikova E, Yu LP, Cheung WS, Dahmen KA, Liaw PK. Plastic dynamics of the Al_{0.5}CoCrCuFeNi high entropy alloy at cryogenic temperatures: Jerky flow, stair-like fluctuation, scaling behavior and non-chaotic state. Appl Phys Lett 2017;111:251905.
- [13] Lu KJ, Chauhan A, Tirunilai AS, Freudenberger J, Kauffmann A, Heilmaier M, Aktaa J. Deformation mechanisms of CoCrFeMnNi high-entropy alloy under low-cycle-fatigue loading. Acta Mater 2021;215:117089.
- [14] Lu KJ, Chauhan A, Walter M, Tirunilai AS, Schneider M, Laplanche G, Freudenberger J, Kauffmann A, Heilmaier M, Aktaa J. Superior low-cycle fatigue properties of CoCrNi compared to CoCrFeMnNi. Scr Mater 2021;194:113667.
- [15] Lu KJ, Knopfle F, Chauhan A, Jeong HT, Litvinov D, Walter M, Kim WJ, Aktaa J. Low-cycle fatigue behavior and deformation mechanisms of a dual-phase Al_{0.5}CoCrFeMnNi high-entropy alloy. Int J Fatigue 2022;163:107075.
- [16] Liu K, Nene SS, Frank M, Sinha S, Mishra RS. Extremely high fatigue resistance in an ultrafine grained high entropy alloy. Appl Mater Today 2019;15:525–30.

- [17] Zhang Y, Wen C, Wang CX, Antonov S, Xue DZ, Bai Y, Su YJ. Phase prediction in high entropy alloys with a rational selection of materials descriptors and machine learning models. Acta Mater 2020;185:528–39.
- [18] Wu LL, Wei GY, Wang G, Wang HY, Ren JL. Creating win-wins from strength-ductility trade-off in multi-principal element alloys by machine learning. Mater Today Commun 2022;32:104010.
- [19] Chang HN, Tao YW, Liaw PK, Ren JL. Phase prediction and effect of intrinsic residual strain on phase stability in high-entropy alloys with machine learning. J Alloys Compd 2022;921:166149.
- [20] Sai NJ, Rathore P, Chauhan A. Machine learning-based predictions of fatigue life for multi-principal element alloys. Scr Mater 2023;226:115214.
- [21] Chen D, Li YZ, Liu K, Li Y. A physics-informed neural network approach to fatigue life prediction using small quantity of samples. Int J Fatigue 2023;166:107270.
- [22] Shukla S, Mishra RS. Excellent high cyclic fatigue properties of a novel ultrafine-grained medium entropy alloy. Mater Sci Eng A 2020;779:139122.
- [23] Kuzminova YO, Firsov DG, Dagesyan SA, Konev SD, Sergeev SN, Zhilyaev AP, Kawasaki M, Akhato IS, Evlashin SA. Fatigue behavior of additive manufactured CrFeCoNi medium-entropy alloy. J Alloy Compd 2021;863:158609.
- [24] Chen YA, Li B, Chen B, Xuan FZ. High-cycle fatigue induced twinning in CoCrFeNi high-entropy alloy processed by laser powder bed fusion additive manufacturing. Addit Manuf 2023;61:103319.
- [25] Kashaev N, Ventzke V, Petrov N, Horstmann M, Zherebtsov S, Shaysultanov D, Sanin V, Stepanov N. Fatigue behaviour of a laser beam welded CoCrFeNiMn-type high entropy alloy. Mater Sci Eng A 2019;766:138358.
- [26] Shams SAA, Jang G, Won JW, Bae JW, Jin H, Kim HS, Lee CS. Low-cycle fatigue properties of CoCrFeMnNi high-entropy alloy compared with its conventional counterparts. Mater Sci Eng A 2020;792:139661.
- [27] Suzuki K, Koyama M, Hamada S, Tsuzaki K, Noguchi H. Planar slip-driven fatigue crack initiation and propagation in an equiatomic CrMnFeCoNi high-entropy alloy. Int J Fatigue 2020;133:105418.
- [28] Picak S, Wegener T, Sajadifar SV, Sobrero C, Richter J, Kim H, Niendorf T, Karaman I. On the low-cycle fatigue response of CoCrNiFeMn high entropy alloy with ultra-fine grain structure. Acta Mater 2021;205:116540.
- [29] Kim YK, Ham GS, Kim HS, Lee KA. High-cycle fatigue and tensile deformation behaviors of coarse-grained equiatomic CoCrFeMnNi high entropy alloy and unexpected hardening behavior during cyclic loading. Intermetallics 2019;111:106486.
- [30] Ghomsheh MZ, Khatibi G, Weiss B, Lederer M, Schwarz S, Steiger-Thirsfeld A, Tikhonovsky MA, Tabachnikova ED, Schafler E. High cycle fatigue deformation mechanisms of a single phase CrMnFeCoNi high entropy alloy. Mater Sci Eng A 2020;777:139034.
- [31] Tian YZ, Sun SJ, Lin HR, Zhang ZF. Fatigue behavior of CoCrFeMnNi high-entropy alloy under fully reversed cyclic deformation. J Mater Sci Technol 2019;35:334-40.
- [32] Lee GT, Won JW, Lim KR, Kang MJ, Kwon HJ, Na YS, Choi YS. Effect of microstructural features on the high-cycle fatigue behavior of CoCrFeMnNi high-entropy alloys deformed at room and cryogenic temperatures. Metals Mater Int 2021;27:593–602.
- [33] Kim YK, Baek MS, Yang S, Lee KA. In-situ formed oxide enables extraordinary high-cycle fatigue resistance in additively manufactured CoCrFeMnNi high-entropy alloy. Addit Manuf 2021;38:101832.
- [34] Liu KM, Komarasamy M, Gwalani B, Shukla S, Mishra RS. Fatigue behavior of ultrafine grained triplex Al_{0.3}CoCrFeNi high entropy alloy. Scr Mater 2019;158:116–20.
- [35] Alagarsamy K, Fortier A, Komarasamy M, Kumar N, Mohammad A, Banerjee S, Han HC, Mishra RS. Mechanical properties of high entropy alloy Al_{0.1}CoCrFeNi for peripheral vascular stent application. Cardiovasc Eng Technol 2016;7:448–54.
- [36] Feng R, Rao Y, Liu CH, Xie X, Yu DJ, Chen Y, Ghazisaeidi M, Ungar T, Wang HM, An K, Liaw PK. Enhancing fatigue life by ductile-transformable multicomponent B2 precipitates in a high-entropy alloy. Nature Commun 2021;12:3588.
- [37] Liu KM, Gwalani B, Komarasamy M, Shukla S, Wang TH, Mishra RS. Effect of nano-sized precipitates on the fatigue property of a lamellar structured high entropy alloy. Mater Sci Eng A 2019;760:225–30.
- [38] Shukla S, Wang TH, Cotton S, Mishra RS. Hierarchical microstructure for improved fatigue properties in a eutectic high entropy alloy. Scr Mater 2018;156:105–9.
- [39] Wang XD, Bai WL, Zhang Z, Wang ZB, Ren XC. Enhanced fatigue resistance of a face-centered-cubic single-phase Al_{0.3}CoCrFeNi high-entropy alloy through planar deformation characteristic. Mater Sci Eng A 2023;862:144499.
- [40] Zhang Y, Ling C. A strategy to apply machine learning to small datasets in materials science. NPJ Comput Mater 2018;4:25.
- [41] Basquin OH. The exponential law of endurance tests. Proc Am Soc Test Mater 1910;10:625–30.
- [42] He L, Wang ZL, Akebono H, Sugeta A. Machine learning-based predictions of fatigue life and fatigue limit for steels. J Mater Sci Technol 2021;90:9-19.
- [43] Lundberg SM, Lee SI. A unified approach to interpreting model predictions. Adv Neural Inf Process Syst 2017;30:4765-74.
- [44] Friedman JH. Greedy function approximation: a gradient boosting machine. Ann Stat 2001;29:1189-232.
- [45] Liu K, Nene SS, Frank M, Sinha S, Mishra RS. Metastability-assisted fatigue behavior in a friction stir processed dual-phase high entropy alloy. Mater Res Lett 2018;6:613–9.
- [46] Chen SY, Li WD, Wang L, Yuan T, Tong Y, Tseng KK, Yeh JW, Xiong QG, Wu ZG, Zhang F, Liu TK, Li K, Liaw PK. Stress-controlled fatigue of HfNbTaTiZr high-entropy alloy and associated deformation and fracture mechanisms. J Mater Sci Technol 2022;114:191–205.